Spectro-electrochemical and DFT studies of a planar Cu(II)-phenolate complex active in the aerobic oxidation of primary alcohols

Maheswari, P.U.; Hartl, F.; Quesada, M.; Buda, F.; Lutz, M.; Spek, A.L.; ... ; Reedijk, J.

Citation

Maheswari, P. U., Hartl, F., Quesada, M., Buda, F., Lutz, M., Spek, A. L., … Reedijk, J. (2011). Spectro-electrochemical and DFT studies of a planar Cu(II)-phenolate complex active in the aerobic oxidation of primary alcohols. *Inorganica Chimica Acta*, *374*(1), 406-414. doi:10.1016/j.ica.2011.03.029

Version:	Publisher's Version
License:	Licensed under Article 25fa Copyright Act/Law (Amendment Taverne)
Downloaded from:	https://hdl.handle.net/1887/3480031

Note: To cite this publication please use the final published version (if applicable).

Inorganica Chimica Acta 374 (2011) 406–414

Contents lists available at ScienceDirect

Inorganica Chimica Acta

journal homepage: www.elsevier.com/locate/ica

Spectro-electrochemical and DFT studies of a planar Cu(II)–phenolate complex active in the aerobic oxidation of primary alcohols

Palanisamy Uma Maheswari [a], František Hartl [b,*], Manuel Quesada [a,1], Francesco Buda [a], Martin Lutz [c], Anthony L. Spek [c], Patrick Gamez [a,1], Jan Reedijk [a,d,*]

[a] Leiden Institute of Chemistry, Leiden University, P.O. Box 9502, 2300 RA Leiden, The Netherlands
[b] Department of Chemistry, University of Reading, Whiteknights, Reading RG6 6AD, UK
[c] Bijvoet Centre for Biomolecular Research, Crystal and Structural Chemistry, Utrecht University, Padualaan 8, 3584 CH Utrecht, The Netherlands
[d] Department of Chemistry, King Saud University, P.O. Box 2455, Riyadh 11451, Saudi Arabia

ARTICLE INFO

Article history:
Available online 13 March 2011

Dedicated to Prof. Dr. Wolfgang Kaim for his significant contribution to coordination chemistry and spectro-electrochemistry

Keywords:
Copper(II)
Galactose oxidase
Primary alcohol oxidation
Magnetic susceptibility
Spectro-electrochemistry
DFT

ABSTRACT

A square-planar compound [Cu(pyrimol)Cl] (pyrimol = 4-methyl-2-*N*-(2-pyridylmethylene)aminophenolate) abbreviated as CuL–Cl) is described as a biomimetic model of the enzyme galactose oxidase (GOase). This copper(II) compound is capable of stoichiometric aerobic oxidation of activated primary alcohols in acetonitrile/water to the corresponding aldehydes. It can be obtained either from Hpyrimol (HL) or its reduced/hydrogenated form Hpyramol (4-methyl-2-*N*-(2-pyridylmethyl)aminophenol; H_2L) readily converting to pyrimol (L^-) on coordination to the copper(II) ion. Crystalline CuL–Cl and its bromide derivative exhibit a perfect square-planar geometry with Cu–O(phenolate) bond lengths of 1.944(2) and 1.938(2) Å. The cyclic voltammogram of CuL–Cl exhibits an irreversible anodic wave at +0.50 and +0.57 V versus ferrocene/ferrocenium (Fc/Fc^+) in dry dichloromethane and acetonitrile, respectively, corresponding to oxidation of the phenolate ligand to the corresponding phenoxyl radical. In the strongly donating acetonitrile the oxidation path involves reversible solvent coordination at the Cu(II) centre. The presence of the dominant Cu^{II}–$L^{\cdot}$ chromophore in the electrochemically and chemically oxidised species is evident from a new fairly intense electronic absorption at 400–480 nm ascribed to a several electronic transitions having a mixed $\pi \rightarrow \pi^*(L^{\cdot})$ intraligand and Cu–Cl $\rightarrow L^{\cdot}$ charge transfer character. The EPR signal of CuL–Cl disappears on oxidation due to strong intramolecular antiferromagnetic exchange coupling between the phenoxyl radical ligand ($L^{\cdot}$) and the copper(II) centre, giving rise to a singlet ground state ($S = 0$). The key step in the mechanism of the primary alcohol oxidation by CuL–Cl is probably the α-hydrogen abstraction from the equatorially bound alcoholate by the phenoxyl moiety in the oxidised pyrimol ligand, Cu–$L^{\cdot}$, through a five-membered cyclic transition state.

Crown Copyright © 2011 Published by Elsevier B.V. All rights reserved.

1. Introduction

The search for efficient oxidation catalysts is increasingly being guided and stimulated by considering the active site structures of metalloenzymes. An example is the fungal enzyme galactose oxidase (GOase) catalysing selectively aerobic oxidation of a wide range of primary alcohols to the corresponding aldehydes, with a concomitant formation of stoichiometric amounts of dihydrogen peroxide by a coupled dioxygen reduction [1–10]. The enzyme is unusual because, in contrast to most copper proteins carrying out multielectron redox reactions at multinuclear Cu(I) ↔ Cu(II) active sites, it uses a single copper centre to carry out a two-electron redox process. Spectroscopic studies of the GOase indicate that the isolated inactive enzyme contains a Cu^{II}–tyrosinate fragment that is converted upon treatment with oxidants into the active form containing a Cu^{II}–tyrosinyl radical pair in the equatorial position [11].

Key evidences for the formulation of the active form include the silent EPR response ascribed to antiferromagnetic exchange coupling between the two $S_{1/2}$ centres, the X-ray absorption edge data indicative of the presence of Cu(II), the resonance Raman data showing diagnostic phenoxyl radical vibrations, and an intense absorption band at $\lambda_{max} = 444$ nm ($\varepsilon_{max} = 5190\ M^{-1}\ cm^{-1}$, GOase), which has been postulated to involve a $\pi \rightarrow \pi^*$ electronic transition of the phenoxyl radical [12–16]. The ability of the mononuclear active site to carry out a two-electron process has been rationalised

* Corresponding authors. Addresses: Department of Chemistry, University of Reading, Whiteknights, Reading RG6 6AD, UK (F. Hartl), Leiden Institute of Chemistry, Leiden University, P.O. Box 9502, 2300 RA Leiden, The Netherlands (J. Reedijk). Tel.: +44 118 378 7695; fax: +44 118 378 6331 (F. Hartl).
E-mail address: f.hartl@reading.ac.uk (F. Hartl).
[1] Present address: ICREA, Universitat de Barcelona, Departament de Quimica Inorganica, 08028 Barcelona, Spain.

0020-1693/$ - see front matter Crown Copyright © 2011 Published by Elsevier B.V. All rights reserved.
doi:10.1016/j.ica.2011.03.029

by a redox cycle between the active Cu^{II}–tyrosinyl unit and the reduced Cu(I) state. The Cu^{II}–tyrosinyl radical moiety is assumed to be directly responsible for the hydrogen atom abstraction from the alcoholate substrate bound in the equatorial position.

The unusual nature of the cysteine-modified Cu^{II}–tyrosinyl radical species, its key role in the enzyme catalysis and the challenge of fully understanding the mechanism of the alcohol oxidation provide a sufficient thrust for undertaking thorough studies of functional models of the active site of the GOase [17,18].

Although a large number of Cu^{II}–phenolate-based structural models of the active and inactive forms of the GOase have been synthesized and spectroscopically characterised [19–27], only a few functional models have been reported so far [6,8,28–30]. Pioneering studies by Kitajima et al. in the mid-1980s have dealt with two tetrahedrally distorted phenolic Schiff-base copper(II) complexes capable of oxidising primary alcohols to corresponding aldehydes in the presence of an excess of alkoxide [31]. One decade later, Stack and co-worker described the use of a functional mononuclear Cu(II) model compound as a catalyst of aerobic oxidation of activated benzyl and allylic alcohols with high TONs, again in the presence of an excess of the base (alkoxide) as co-catalyst [32]. More recently, Wieghardt and co-workers reported a unique mononuclear 2,2′-thiobis(phenolato) triethylamine copper(II) compound that oxidised both primary and secondary alcohols to the corresponding aldehydes and ketones, respectively, and/or to 1,2-glycol derivatives [33–35]. The selective aerobic oxidation of primary alcohols (but not methanol) was achieved with a related Cu(II) compound containing two-electron-reducible iminosemiquinone ligands and NEt_3. Mononuclear copper complexes with sterically demanding Schiff-base ligands were applied by Stack and co-workers in the stoichiometric conversion of benzyl alcohol to benzaldehyde in the presence of a base and an oxidant [36]. Itoh et al. performed the same oxidation using mononuclear copper complexes bearing thioether-linked phenolic ligands. The importance of a reducible copper(II) site and the interconversion between the phenol and phenoxyl radical ligand redox forms in the two-electron oxidation of alcohols were clearly demonstrated by comparison with analogous but inactive Zn(II) complexes [6,37–40].

Herein, we report on a square-planar copper(II) compound [Cu(pyrimol)Cl] (pyrimol = 4-methyl-2-*N*-(2-pyridylmethylene)-aminophenolate, L^-; Fig. 1b) capable of oxidising primary alcohols to corresponding aldehydes. This functional model of the GOase has been obtained from $CuCl_2$ and Hpyrimol (HL; Fig. 1a). The reduced and hydrogenated form of the ligand, Hpyramol (4-methyl-2-*N*-(2-pyridylmethyl)aminophenol, H_2L) can also be used, readily converting to pyrimol (L^-) upon coordination to the copper(II) ion, as communicated elsewhere [41]. The corresponding bromide compound, CuL–Br, has also been prepared and structurally fully characterised.

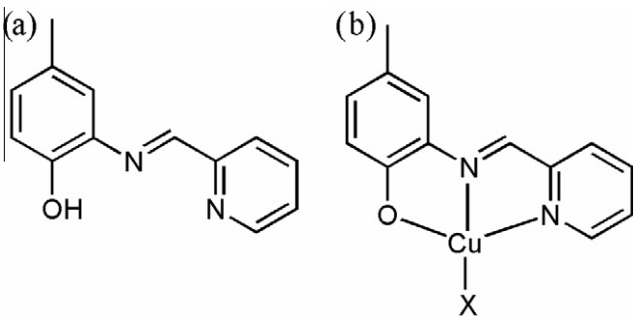

Fig. 1. Schematic molecular structures of (a) Hpyrimol (HL) and (b) [Cu(pyrimol)X] (CuL–X, X = Cl and Br).

2. Experimental

2.1. Materials

All chemicals for the syntheses were used as received without further purification. The ligand (4-methyl-2-*N*-(2-pyridylmethyl)aminophenol (Hpyramol)) was obtained in a single-step reaction as previously reported [42,43]. Dichloromethane and acetonitrile (Acros) for spectro-electrochemistry were freshly distilled from CaH_2 under a dry nitrogen atmosphere. The supporting electrolyte Bu_4NPF_6 (Aldrich) was recrystallized twice from absolute ethanol and dried overnight under reduced pressure at 80 °C. Ferrocene, cobaltocenium hexafluoridophosphate and tris(4-bromophenyl)aminium hexachloridoantimonate (all Aldrich) were used as received.

2.1.1. Synthesis of 4-methyl-2-N-(2-pyridylmethylene)aminophenol (Hpyrimol)

A solution of 10.7 g (0.1 mol) of picolinaldehyde in methanol (75 mL) was added, under constant stirring, to a solution of 12.4 g (0.1 mol) of 2-amino-4-methylphenol in methanol (50 mL) dried on molecular sieves (4 Å). The reaction mixture was refluxed for 2 h at 70 °C. Next, methanol was evaporated under a reduced pressure. The deep green residue was redissolved in CH_2Cl_2 (200 mL), filtered and layered with *n*-hexane (200 mL). The resulting bilayer was left at −20 °C to promote crystallization of the pure compound. After 2 days, bright yellow crystals were obtained. The crystals were collected and washed with diethyl ether, and subsequently dried under argon. Yield: 53%. ^{1}H NMR ($CDCl_3$): δ 8.81 (s), 8.72 (d), 8.20 (d), 7.82 (t), 7.37 (m), 7.25 (d), 7.2 (s), 7.1 (s), 7.06 (d), 6.90 (d), 2.31 (s) ppm.

2.1.2. Synthesis of [Cu(pyrimol)X]·H_2O (X = Cl, Br)

As an alternative to the literature procedure [41] [Cu(pyrimol)Cl]·H_2O was prepared by layering a solution of Hpyrimol in THF and an aqueous solution of $CuCl_2$. A solution of $CuCl_2{\cdot}2H_2O$ (127.3 mg, 0.747 mmol), in 15 mL H_2O was added dropwise to a solution of Hpyrimol (212.2 mg, 1 mmol) in 15 mL water. Dark red crystals were formed in 34% yield. *Anal.* Calc. for $C_{13}H_{11}ClCuN_2O{\cdot}H_2O$ (M_w: 328.24): C, 47.57; H, 3.99; N, 8.53. Found: C, 47.54; H, 4.36; N, 8.50%. The analogous bromide compound was prepared similarly and obtained as dark red needles. Yield: 19%. *Anal.* Calc. for $C_{13}H_{11}BrCuN_2O{\cdot}H_2O$ (M_w: 372.70): C, 47.57; H, 3.99; N, 8.53. Found: C, 47.52; H, 3.96; N, 8.55%. [Cu(pyrimol)Br]·H_2O is isomorphous to [Cu(pyrimol)Cl]·H_2O prepared from the ligands Hpyramol or Hpyrimol (see below).

2.2. X-ray crystallography

Reflections were measured on a Nonius Kappa CCD diffractometer with a rotating anode (graphite monochromator, λ = 0.71073 Å) up to resolution of $(\sin\theta/\lambda)_{max}$ = 0.65 Å^{-1}. Intensities were integrated with EvalCCD [44], using an accurate description of the experimental setup for the prediction of the reflection contours. The structures were refined with SHELXL-97 [45] against F^2 of all reflections. Non-hydrogen atoms were refined with anisotropic displacement parameters. All hydrogen atoms were located in the difference Fourier map. The hydrogen atoms at C1 and in the water molecule were refined freely with isotropic displacement parameters; all other hydrogen atoms were refined with a riding model. Geometry calculations and checking for higher symmetry was performed with the PLATON program [46].

2.3. [Cu(pyrimol)Cl]·H_2O

$C_{13}H_{11}ClCuN_2O(H_2O)$, M_w = 328.24 g mol^{-1}, dark red needle, 0.60 × 0.09 × 0.06 mm^3, triclinic, $P\bar{1}$ (No. 2), a = 6.6991(4), b = 8.7519(4), c = 12.2726(7) Å, α = 100.042(2), β = 100.131(2), γ = 110.053(1)°, V = 643.60(6) Å^3, Z = 2, D_x = 1.694 g cm^{-3}, μ = 1.90 mm^{-1}. In total 11,897 reflections were measured at T = 150 K; 2945 reflections were unique (R_{int} = 0.0178). An absorption correction based on multiple measured reflections was applied using the program SADABS [47] (0.34–0.89 correction range). The structure was solved with the program DIRDIF-99 [48] using automated Patterson Methods and found to be similar to the room-temperature structure of the compound starting differently prepared from Hpyramol [41]. The 185 parameters were refined with no restraints. $R1/wR2$ [$I > 2\sigma(I)$]: 0.0291/0.0799. $R1/wR2$ [all reflections]: 0.0323/0.0819. S = 1.165. Residual electron density ranges between −0.44 and 0.68 e/Å^3.

2.4. [Cu(pyrimol)Br]·H_2O

$C_{13}H_{11}BrCuN_2O(H_2O)$, M_w = 372.70 g mol^{-1}, dark red needle, 0.78 × 0.04 × 0.04 mm^3, triclinic, $P\bar{1}$ (No. 2), a = 6.7419(3), b = 8.8574(6), c = 12.2550(6) Å, α = 101.696(2), β = 97.836(2), γ = 110.233(2)°, V = 655.21(6) Å^3, Z = 2, D_x = 1.889 g cm^{-3}, μ = 4.71 mm^{-1}. In total 13,266 reflections were measured at T = 150 K; 2981 reflections were unique (R_{int} = 0.0837). The crystal appeared to be non-merohedrally twinned with a twofold rotation about the crystallographic a-axis as twin operation. This twin operation was taken into account during the integration of the intensities and the refinement as a HKLF5 refinement [49]. An analytical absorption correction was applied (0.23–0.86 correction range). The coordinates of the isomorphous [Cu(pyrimol)Cl]·H_2O were taken as starting model for the refinement. The 186 parameters were refined with no restraints on all unique data. $R1/wR2$ [$I > 2\sigma(I)$]: 0.0414/0.1041. $R1/wR2$ [all reflections]: 0.0546/0.1127. S = 1.152. The twin fraction refined to 0.563(3). Residual electron density ranges between −0.75 and 1.07 e/Å^3.

2.5. Experimental procedures and methods

The oxidation of primary alcohols was carried out in air within a 100 mL three-necked round-bottom flask. Typically, the aerated alcohol (2 mmol) was diluted with acetonitrile (15 mL) and the base, ^{t}BuOK dissolved in H_2O (5 mL), was added. The solution was magnetically stirred for 5 min. $CuCl_2$ (2 mmol) and Hpyramol or Hpyrimol (2 mmol) were added stepwise at this stage, and the reaction solution turned dark red. Crystalline CuL–Cl can also be used instead of the in situ $CuCl_2$–Hpyramol/Hpyrimol combination. Samples for analyses were collected at regular intervals. The organic layer was extracted with diethyl ether/H_2O (1:1, 10 mL), and the extract was concentrated to 1 mL. The conversion (%) was then determined by gas chromatography, using co-injected 1,2-dibromobenzene as an internal standard. The GC analysis was carried out using a Hewlett–Packard 5890 Series GC (CP-Sil-5 CB WCOT Fused Silica capillary column, 50 m × 0.25 mm inside diameter (i.d.), 0.25 μm film thickness) with dihydrogen carrier gas. The products of the reaction were determined by comparison with the commercially available carbonyl compounds.

Elemental analyses (C, H, N) were carried out on a Perkin-Elmer 2400 series II analyser. X-band EPR measurements of a crystalline sample of CuL–Cl were performed at 77 K, Bruker-EMXplus spectrometer (field calibrated with DPPH (g = 2.0036)). Magnetic susceptibility measurements at 5–300 K were carried out using a Quantum Design MPMS-5S SQUID magnetometer, in a 1 kG applied field. Data were corrected for the experimentally determined contribution of the sample holder. The selective one-electron oxidation of CuL–Cl with tris(4-bromophenyl)aminium hexachloridoantimonate (E^o = +0.70 V versus Fc/Fc$^+$) [50] was performed in acetonitrile and dichloromethane under argon on UV–Vis monitoring. Acetonitrile was evaporated under reduced pressure to give a dark-green powder used for the magnetic measurements. Corrections were applied for the diamagnetic responses of the compound, as estimated from the Pascal constants [51].

Cyclic voltammetry of 10^{-3} M CuL–Cl in a single-compartment cell was carried out with an Autolab PGSTAT10 potentiostat (Eco Chemie) controlled by the GPES4 software, or with an EG&G PAR Model 283 potentiostat operated with the PAR Power CV® software. The dichloromethane and acetonitrile solutions contained 10^{-1} M Bu_4NPF_6 as the supporting electrolyte. The three-electrode system consisted of a carefully polished Pt disc working electrode, a platinum auxiliary electrode, and an Ag/AgCl reference electrode. The voltammetric response of the standard ferrocene/ferrocenium (Fc/Fc$^+$) couple was found in this system at +0.55 V versus Ag/AgCl. Cobaltocenium hexafluoridophosphate was added as internal potential standard (−1.33 V versus Fc/Fc$^+$) when an Ag wire was used as a pseudo-reference electrode.

The air-tight UV–Vis and EPR spectro-electrochemical cells employed for the in situ oxidation of 2 mM CuL–Cl at variable temperatures have been described in detail elsewhere [52–55]. The electrode potential was controlled during the in situ electrolyses by a PA4 potentiostat (EKOM, Polná, Czech Republic). UV–Vis spectra were recorded with a HP 8453 diode array spectrophotometer, and the X-band EPR spectra with a Varian Century E-104A spectrometer.

Density functional theory (DFT) calculations were performed with the GAUSSIAN 03 package [56]. We used the hybrid B3LYP exchange and correlation functional [57,58] and a 6-311G(d,p) basis set. All calculations are spin-unrestricted. The choice of this hybrid functional is important to obtain accurate results both for the structural and absorption properties of the CuL–Cl complex. The DFT-optimised geometry of the compound is in excellent agreement with the corresponding X-ray crystal structure data (see Table S1 in Supplementary material). Time-dependent DFT calculations (TD-DFT) were performed with the same functional and basis set to evaluate electronic absorption spectra. The geometry of all complexes was optimised prior to the TD-DFT calculations. TD-DFT calculations were also performed in the presence of a solvent treated within the Polarizable Continuum Model (PCM) [59]. The ionisation potential was estimated by a ΔSCF calculation, i.e. by taking the difference in the total energy of the complex before and after its one-electron oxidation.

3. Results and discussion

3.1. Crystal structures

The compounds [Cu(pyrimol)X] (X = Cl, Br) can be obtained both from the Hpyramol (H_2L) and Hpyrimol (HL) ligands by a bilayer method, with the ligand dissolved in THF or ethyl acetate and the Cu(II) salt in H_2O. Crystals of the product appear typically within 2 days at 293–273 K. The compounds reported herein, obtained from the bilayer containing the Hpyrimol ligand and $CuCl_2$/$CuBr_2$ salts, are isomorphous to CuL–Cl prepared earlier [41] from $CuCl_2$ and Hpyramol that readily dehydrogenates upon coordination to give the pyrimol ligand, L^-.

The coordination geometries of Cu(II) are perfectly square planar, with the NNO pyrimol and halide (Cl/Br) coordination. Views of CuL–X (X = Cl, Br) are presented in Fig. 2 (for X = Br; bond parameters are in the caption), Fig. S1 (for X = Cl) and Figs. S2 and S3 for the packing diagrams of both compounds. The structural parameters regarding hydrogen bonds are collected in Table 1. The

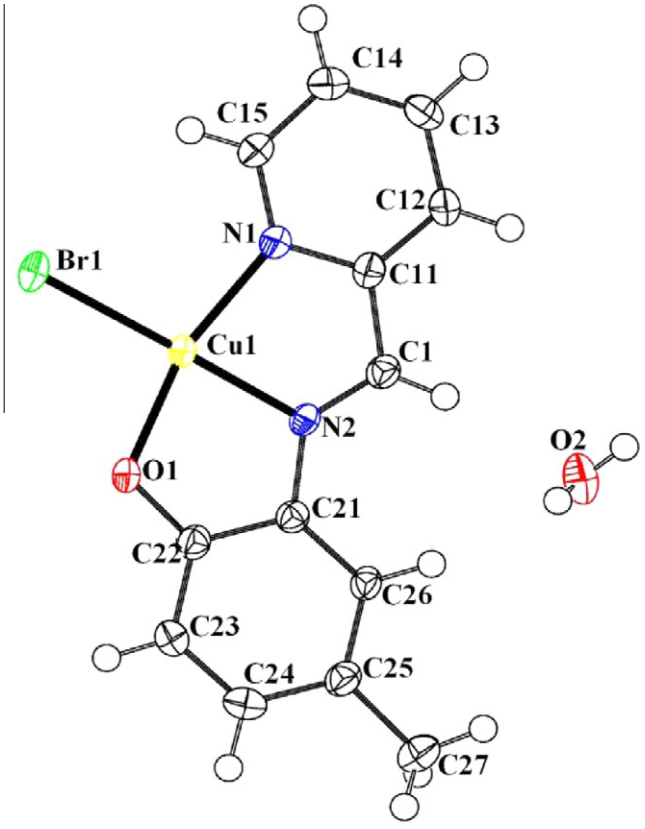

Fig. 2. Molecular structure of [Cu(pyrimol)Br]·H_2O (50% probability level). Selected bond lengths (Å) and angles [°]: Cu1–O1 1.938(3), Cu1–Br1 2.3553(6), Cu1–N1 2.018(4), Cu1–N2 1.965(3); O1–Cu1–Br1 95.53(9), Br1–Cu1–N1 100.57(10), N1–Cu1–N2 80.54(14), N2–Cu1–O1 83.36(13).

Table 1
Hydrogen-bonding parameters for [Cu(pyrimol)X]·H_2O (X = Cl, Br).

D–H···A	D–H (Å)	H···A (Å)	D···A (Å)	D–H···A (°)
[Cu(pyrimol)Cl]·H_2O				
O2–H2A···O1^{i}	0.83(4)	2.04(4)	2.830(3)	160(3)
O2–H2B···O1^{ii}	0.75(4)	2.10(4)	2.832(3)	165(4)
[Cu(pyrimol)Br]·H_2O				
O2–H2A···O1^{i}	0.75(7)	2.13(7)	2.857(5)	162(7)
O2–H2B···O1^{ii}	0.76(6)	2.10(6)	2.842(5)	162(5)

Symmetry operations: i–x, $y-1$, z; ii–$2-x$, $1-y$, $1-z$.

compound CuL–Cl has already been reported by some of us to cleave DNA oxidatively without any specific reductant added [41]. This process has revealed the ability of CuL–Cl to form reactive radical species and to abstract hydrogen atoms from a sugar substrate. The oxidation of primary alcohols to corresponding aldehydes under stoichiometric conditions is discussed in the light of spectroscopic and electrochemical properties of CuL–Cl, with references to the GOase catalytic cycle.

Two-dimensional hydrogen-bonding patterns were found between the non-coordinated H_2O molecules present in the lattice and the adjacent phenolate oxygen from the Cu-pyrimol compound.

3.2. Cyclic voltammetry

In the anodic region, the cyclic voltammogram of CuL–Cl shows an irreversible wave (O1) at $E_{p,a}$ = +0.50 V versus Fc/Fc$^+$ in dichloromethane (Fig. 3) and +0.57 V versus Fc/Fc$^+$ in acetonitrile. These

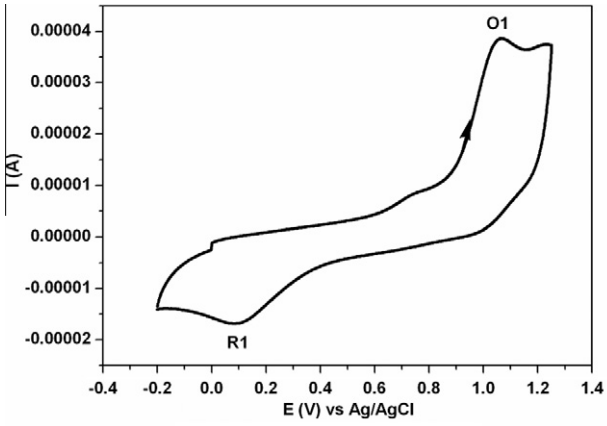

Fig. 3. Cyclic voltammogram of 10^{-3} M CuL–Cl in the anodic region. Conditions: Freshly polished Pt working electrode (apparent surface area of 0.312 cm^2), v = 100 mV s^{-1}, dichloromethane/10^{-1} M Bu_4NPF_6, room temperature.

values were confirmed against the standard cobaltocenium hexafluoridophosphate used as an internal reference. The oxidised species then reduces back on the reverse scan in dichloromethane at $E_{p,c}$ = −0.34 V versus Fc/Fc$^+$ (0.14 mm^2 Pt microdisc) or −0.45 V versus Fc/Fc$^+$ (0.312 cm^2 Pt disc; the irreversible cathodic wave R1 in Fig. 3) and in acetonitrile at −0.15 V versus Fc/Fc$^+$ (0.14 mm^2 Pt microdisc). The same cathodic wave was indeed also observed in the cyclic voltammogram recorded after oxidation of [CuL–Cl] with 1 equiv $(4\text{-}BrC_6H_4)_3N^+SbCl_6^-$. These electrode potential values for the irreversible redox reactions correspond to the scan rate v = 100 mV s^{-1}. The significant solvent dependence of the reduction potential R1 points to the coordination of acetonitrile molecules to the oxidised form of CuL–Cl. To prove this assumption, the voltammetric cycle of CuL–Cl in acetonitrile recorded at v = 500 mV s^{-1} was interrupted for 10 s beyond the anodic wave O1 to accumulate the oxidised product at the electrode surface; the scan direction was then reversed back beyond the cathodic wave R1 of the oxidised product and switched again anodically without interruption. Three complete redox cycles were recorded in this way. Importantly, the back reduction of the oxidised product at R1 forms a new neutral species that oxidises 460 mV less positively than CuL–Cl; the anodic wave O1 of the parent complex becomes indeed significantly smaller compared to the initial forward scan. The new anodic wave was not observed in dichloromethane. The cyclovoltammetric results indicate axial coordination of donating acetonitrile to planar [CuL·–Cl]$^+$. In dichloromethane, oxidised [CuL·–Cl]$^+$ is assumed to coordinate weakly a water molecule coming from crystals of parent [Cu(pyrimol)Cl]·H_2O (see Section 2) and from the electrolyte [60]. The anodic wave O1 of CuL–Cl and the cathodic wave R1 of Fig. 3, hence do not belong to the same (quasireversible) redox couple. The back reduction of the five-coordinate oxidised species leads to the recovery of parent CuL–Cl. For [CuL·–Cl(MeCN)]$^+$ the corresponding neutral transient CuL–Cl(MeCN) is readily detectable on the sub-second voltammetric time scale. It is important to note that the potential difference of 0.46 eV between the oxidations of CuL–Cl and short-lived CuL–Cl(MeCN) agrees exactly with the difference in the ionisation potentials of the two complexes (0.44 eV) obtained from DFT calculations (see below).

3.3. UV–Vis spectro-electrochemistry

The UV–Vis spectrum of CuL–Cl in dichloromethane shows prominent absorption bands at 561, 361, 300 and 238 nm. These bands become replaced during the oxidation within an OTTLE cell

at the O1 electrode potential by new absorptions at 440, 343 and 271 nm, as shown in Fig. 4. Due to the significant involvement of the pyrimol ligand (see below), it is not surprising that the lowest-energy band is strongly affected by the largely pyrimol-based oxidation, producing a phenoxyl radical species [61] that strongly absorbs at λ_{max} = 435 nm (ε_{max} = 5750 M^{-1} cm^{-1}, Fig. 4).

In acetonitrile, the parent compound absorbs in the visible region prominently at 541 nm and the oxidised product $[CuL^{\cdot}–Cl(MeCN)]^+$ at 407 nm. The thin-layer cyclic voltammograms recorded during the in situ oxidation (v = 2 mV s^{-1}) were indeed very close to the conventional scans (cf. Fig. 3), which supports the assignment. The back reduction of the phenoxyl radical product at the R1 wave led to ca 80% reappearance of the UV–Vis spectrum of the starting CuL–Cl species.

In pure dichloromethane, acetonitrile and acetonitrile/H_2O 3:1 (v/v) without the electrolyte, the maximum of the visible absorption of CuL–Cl shifts from 566 to 540 and 488 nm, respectively; the dipole moment is likely to change for a phenolate-to-imino-pyridine intramolecular charge transfer in this region (see below).

One-electron oxidation of CuL–Cl in dichloromethane at room temperature with $(4\text{-}BrC_6H_4)_3N^+SbCl_6^-$ gives in steps a fully stable product absorbing at 438 nm (Fig. 5a), most probably identical to that observed during the in situ spectro-electrochemical experiment. In dry acetonitrile, the one-electron-oxidised product is also stable, but absorbing at 481 nm (Fig. 5b). Unfortunately, we did not succeed to crystallize the oxidised complex for X-ray diffraction analysis, despite several attempts. It cannot be excluded that $[CuL^{\cdot}–Cl(MeCN)]^+$ is sufficiently stable only in the excess of acetonitrile.

Addition of N_2-saturated water to the acetonitrile solution of $[CuL^{\cdot}–Cl(MeCN)]^+$ causes slow disappearance of the complex. As noted above, parent CuL–Cl is stable in aqueous acetonitrile. When monitoring the titration of the activated primary alcohol species (deprotonated with NaOH in H_2O; see Table 3) with CuL–Cl in acetonitrile/H_2O 3:1 (v/v) at room temperature by UV–Vis spectroscopy, the decreasing visible absorption of parent CuL–Cl is an indirect evidence for the conversion of the pyrimol ligand to the oxidised phenoxyl radical species caused by the substrate (alcoholate) binding to CuL–Cl. Compound CuL–Cl is inert at low temperature (−20 °C) toward the alcohol oxidation and shows no UV–Vis spectral changes. In order to partly elucidate the mechanism of the alcohol oxidation, attempts were made to prove the formation of H_2O_2 during the reaction, using the 'Fox Assay' [62]. However, no H_2O_2 was detected. The side product of the primary alcohol to aldehyde oxidation is therefore assumed to be H_2O or a non-diffusible peroxido species, under stoichiometric conditions.

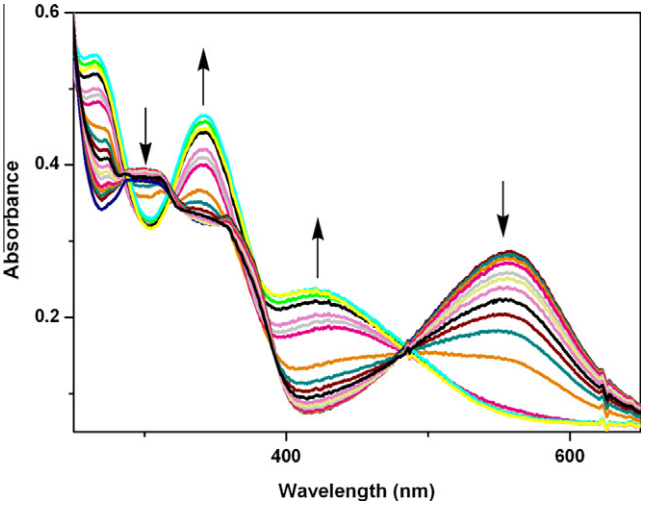

Fig. 4. UV–Vis spectral changes accompanying the oxidation of CuL–Cl in DCM/Bu_4NPF_6 to a phenoxyl radical species at the anodic potential O1. Conditions: Pt minigrid anode, OTTLE cell, room temperature.

3.4. EPR spectroscopy

The EPR spectrum of CuL–Cl in dichloromethane shows at room temperature a well-resolved isotropic signal with a slightly decreasing line width in a stronger magnetic field, which appears as typical for d^9 Cu(II) (Fig. 6, A_{av} = 82.5(5) G, g_{av} = 2.107(1); a simulated spectrum for these parameters in given in Fig. S4). More precisely, the Mulliken analysis has revealed 63% of the spin density on the Cu centre, the rest residing on the four coordinated donor atoms (Cl, N1, N2, O) (cf. Fig. 9). A broadened axial spectrum was observed for a frozen solution of CuL–Cl at 77 K, with no clear anisotropy and hyperfine splitting resolved (g = 2.11(1); spectrum not shown).

As a result of the stoichiometric one-electron oxidation of CuL–Cl with $(4\text{-}BrC_6H_4)_3N^+SbCl_6^-$ the deep red colour of the parent complex in dichloromethane turned dark green (see Fig. 5a). The EPR spectrum of the solution containing oxidised $[CuL^{\cdot}–Cl]^+$ (likely stabilized by coordination of residual water) is completely silent, pointing to the formation of the radical phenoxyl ligand antiferromagnetically coupled to the Cu(II) centre [63]. In situ anodic spectro-electrochemistry with CuL–Cl in dichloromethane at −40 °C led to the same result. The EPR signal of CuL–Cl, which disappeared at the anodic wave O1, was fully recovered at the

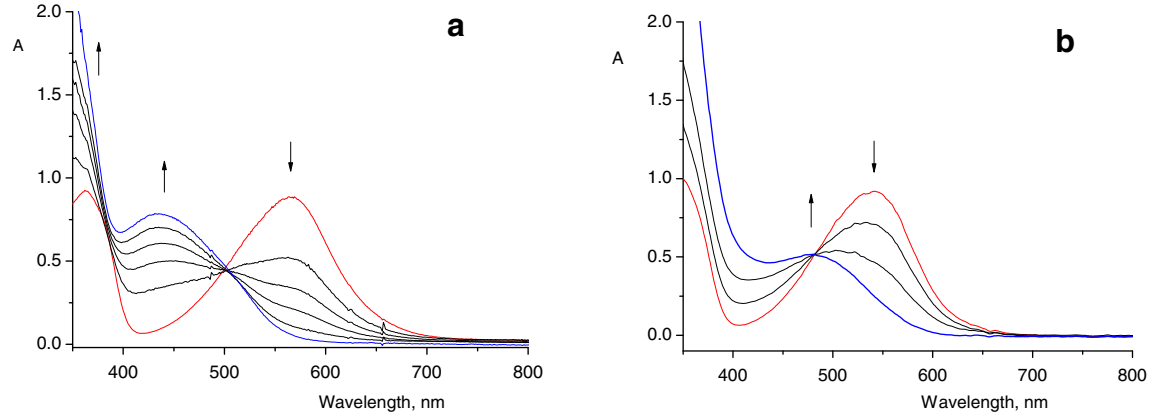

Fig. 5. UV–Vis spectral changes accompanying the stepwise one-electron oxidation of CuL–Cl to a phenoxyl radical species in dichloromethane (a) and acetonitrile (b), using $(4\text{-}BrC_6H_4)_3N^+SbCl_6^-$.

cathodic wave R1 (Fig. 3). This result excludes any extensive irreversible change in the chemical composition induced by the oxidation of the parent compound, e.g., dissociation of the chloride ligand. This behaviour is also in agreement with the magnetic susceptibility data presented in the following section.

3.5. Magnetic behaviour

Magnetic susceptibility measurements were carried out with a crystalline sample of CuL–Cl at variable temperature. The $\chi_M T$ value is 0.393 $cm^3\ mol^{-1}\ K$ at room temperature (Fig. 7, circles), which is close to the value for a single free electron ($\chi_M T$ = 0.375 $cm^3\ mol^{-1}\ K$, g = 2.0023). The value remains almost unchanged till very low temperatures ($T \sim 50$ K), where a small decrease is observed. These data are indicative of very weak antiferromagnetic interactions between the paramagnetic Cu(II) centres in the lattice. On the other hand, the product obtained by the chemical one-electron oxidation of CuL–Cl with $(4\text{-}BrC_6H_4)_3N^+SbCl_6^-$ in acetonitrile is diamagnetic (throughout the same temperature range (5–300 K)), in agreement with the absent EPR signal (see above). No remainders of any non-oxidised sample were observed. Further analysis of $[CuL^{\cdot}\text{–}Cl(MeCN)]^+$ was carried out by density functional theory (DFT) calculations.

3.6. DFT and TDDFT study of CuL–Cl and one-electron-oxidised $[CuL^{\cdot}\text{–}Cl]^+$

DFT calculations were carried out to characterise the CuL–Cl compound and its EPR silent oxidised state $[CuL^{\cdot}\text{–}Cl]^+$, respectively $[CuL^{\cdot}\text{–}Cl(MeCN)]^+$. The geometrical structure of the CuL–Cl compound is in a very good agreement with the available X-ray data (see Table S1; Cartesian coordinates of the optimised complex are given in Supplementary material).

In Table S2 (Supplementary information), we report orbital energies and localisation of frontier molecular orbitals (MOs) of CuL–Cl and other close-lying orbitals relevant for the assignment of major electronic transitions in this complex (Table 2). The ground state of CuL–Cl is a doublet with one excess α electron. Fig. 9 shows the spin density obtained as the difference between the α and β electron densities. The HOMO α and HOMO β (79α and 78β, respectively) of CuL–Cl are very close in energy and consist of a π orbital largely localised on the pyrimol ligand, in particular on the phenolate oxygen and aromatic ring, and to some extent also on the imino nitrogen (see Fig. 9 and Table S2). The singly occupied σ* HOMO-1 α (78α) is about 1.0 eV lower in energy than the HOMO and is largely localised on the Cu–Cl moiety, with strong contributions from all three donor heteroatoms of the pyrimol ligand (Fig. 9 and Table S2).

As shown in Fig. 5, the UV–Vis spectra of CuL–Cl feature a dominant lowest-energy absorption band at 566 nm in dichloromethane and 540 nm in acetonitrile. In order to rationalise the solvatochromic shifts in these spectra and the nature of the corresponding electronic transitions, we performed TD-DFT calculations for CuL–Cl in vacuum and in the presence of a solvent treated

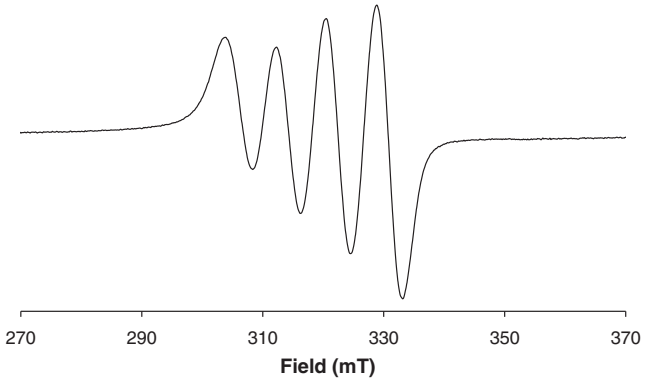

Fig. 6. X-band EPR spectrum of [CuL–Cl] in dichloromethane at room temperature; g = 2.107, A_{iso} = 8.25 mT. The corresponding simulated spectrum is shown in Fig. S4.

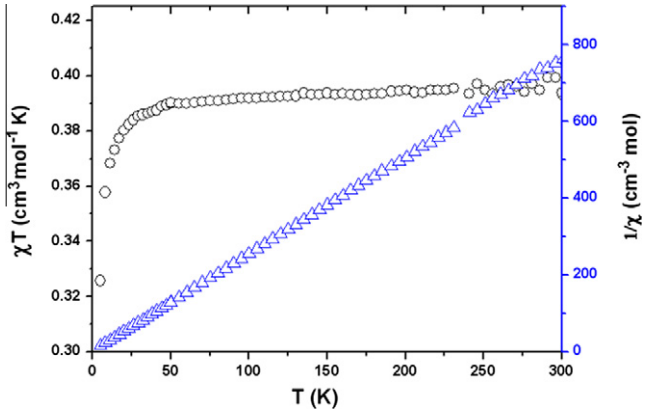

Fig. 7. The plots $\chi_M T$ and $1/\chi_M$ vs. T obtained for the compound [CuL–Cl].

Table 2
TD-DFT computed excitation energies E and oscillator strengths f for electronic transitions (E.T.) in CuL–Cl.

E (eV) (λ, nm)	f[a]	E.T.[b]	Weight[c] (%)
CuL–Cl			
2.207 (562)	0.170	79α → 80α	37
		78β → 79β	37
		70β → 80β	10
2.279 (544)	0.041	70β → 80β	69
3.431 (361)	0.286	75α → 80α	39
		75β → 79β	41

[a] Only the excitation energies with an oscillator strength larger than 0.01 are reported.
[b] Electronic transitions from occupied to virtual MOs. Note that in [CuL–Cl] there are 79α electrons and 78β electrons.
[c] For each excitation energy, the corresponding most relevant molecular orbital transitions are indicated with the relative weight.

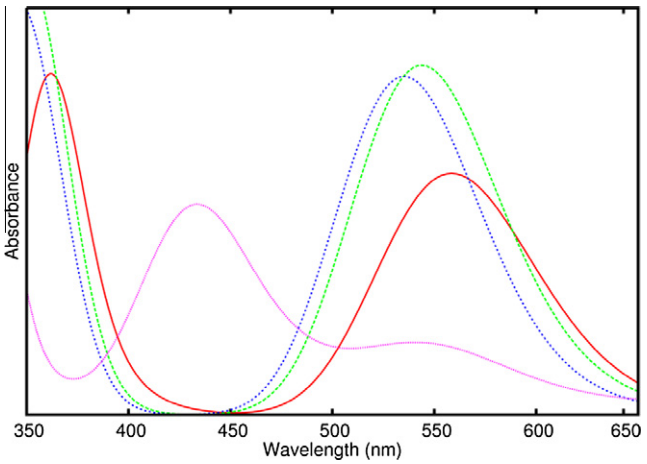

Fig. 8. TDDFT simulated UV–Vis absorption spectra of parent CuL–Cl in vacuum (red, full line), in dichloromethane (green, dashed line), in acetonitrile (blue, dotted line) and the one-electron oxidised species $[CuL^{\cdot}\text{–}Cl]^+$ in dichloromethane (purple, densely dotted line). (For interpretation of the references to colours in this figure legend, the reader is referred to the web version of this paper.)

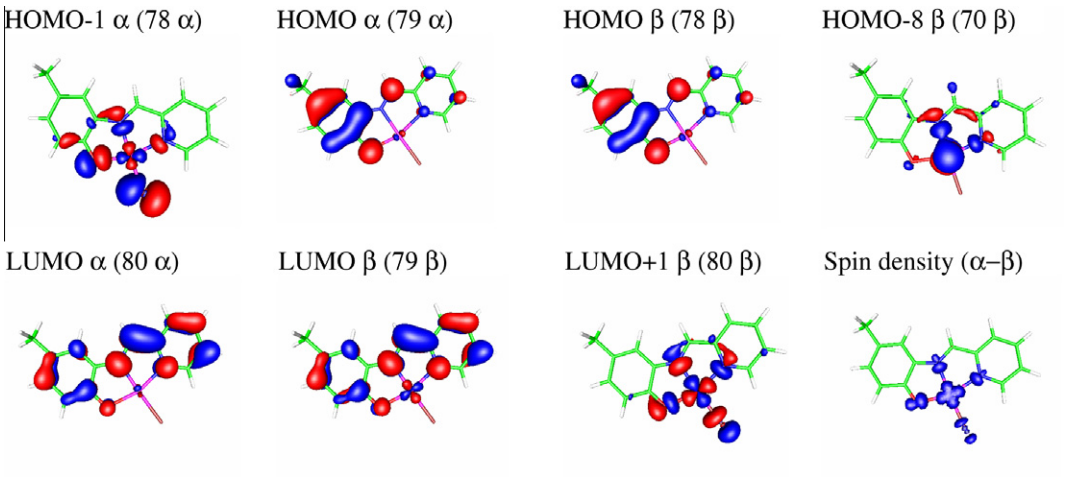

Fig. 9. Molecular orbitals of CuL–Cl relevant for the calculated electronic transitions beyond the absorption peak at 562 nm, and the spin density delocalisation in the complex.

within the PCM method. To simulate the absorption spectra we have considered a superposition of Gaussian peaks centred at the calculated excitation energies, with a height equal to the oscillator strength and a width of 0.15 eV. In Table 2, we report the calculated excitation energies and the corresponding oscillator strengths in vacuum.

The theoretically predicted UV–Vis spectrum of the CuL–Cl compound in vacuum shows two peaks at 562 and 361 nm, in good agreement with the experimental spectrum (see Figs. 4 and 8 for comparison). The lowest-energy excitation at 562 nm arises predominantly from the HOMO(α,β) to LUMO(α,β) electronic transition, which can be described as a π–π*(pyrimol) intraligand or phenolate-to-iminopyridine intramolecular charge transfer transition (see Table 2 and Fig. 9). The lowest-energy absorption band for the parent complex CuL–Cl is predicted to shift to 544 and 535 nm in the presence of the dichloromethane and acetonitrile solvents, respectively. The shift to a higher energy in acetonitrile compared to dichloromethane is consistent with the experimental data shown in Fig. 5, indicating that TD-DFT with the implicit solvent model is able to capture the observed solvatochromic shift (see Fig. 8).

Upon oxidation of the CuL–Cl compound, one electron is expected to be removed from the HOMO, giving rise to a biradicaloid state with two unpaired electrons (in the HOMO and HOMO-1), which can be either ferromagnetically (triplet state) of antiferromagnetically (singlet state) coupled. According to the EPR analysis, the oxidised state is EPR silent and characteristic of an antiferromagnetic coupling (see above). The triplet state would also contrast the diamagnetic nature of the oxidised species. However, when performing the unrestricted DFT/B3LYP calculation on the singlet state of the oxidised complex, the unpaired electron from the HOMO-1 α is removed, resulting in the formation of a cationic singlet state, $[CuL–Cl]^+$ ($S = 0$), with no biradical character. The failure of unrestricted DFT in this case is not surprising due to the intrinsically single determinant nature of the DFT wave function: the biradical singlet state of $[CuL^{\cdot}–Cl]^+$ needs a multi-configuration approach to be described properly, and further theoretical calculations on this issue are planned in the near future. Here, we look instead at the triplet state of $[CuL^{\cdot}–Cl]^+$, which, although not corresponding with the experimentally observed state, carries the correct biradical character (with the two unpaired electrons having parallel spin) and can provide some insight into the nature of the new visible electronic transition. In Fig. 8 we show the calculated electronic absorption spectrum of $[CuL^{\cdot}–Cl]^+$ in dichloromethane in the triplet state. A new absorption band is emerging at around 440 nm, consistently with the experiment. The main electronic transitions responsible for this absorption have a mixed $\pi \rightarrow \pi^*(L^{\cdot})$ intraligand and $Cu–Cl \rightarrow L^{\cdot}$ charge transfer character (see Fig. S5 in Supplementary information). A residual band of lower intensity is also observed at 550 nm, differently from the experimental spectrum. This might be an artefact of the TD-DFT description and another argument for further theoretical investigations.

The UV–Vis spectrum of $[CuL^{\cdot}–Cl]^+$ in the triplet state was also evaluated in acetonitrile. At the same time we considered the axial coordination of a solvent molecule in $[CuL^{\cdot}–Cl(MeCN)]^+$, as indicated by the spectro-electrochemical data. The calculated spectra in these two cases are very similar to the spectrum in Fig. 8 (purple line), showing no significant shift in the position or change in the intensity of the absorption band at 440 nm.

The calculated ionisation potentials for CuL–Cl, CuL–Cl(MeCN), and $[CuL–MeCN]^+$ complexes reach the values of 7.49, 7.05, and 10.33 eV, respectively. Thus, the formation of the pentacoordinate complex $[CuL^{\cdot}–Cl(MeCN)]^+$ is further supported by the DFT results since the anodic potential difference of ca. 0.45 eV between the oxidations of CuL–Cl and short-lived CuL–Cl(MeCN) (see above) corresponds well with the difference in the ionisation potential between the two complexes (0.44 eV) due to the axial acetonitrile coordination. The formation of the oxidised species $[CuL^{\cdot}–MeCN]^{2+}$ can be also discarded on the basis of the much higher computed ionisation energy.

3.7. Oxidation of primary alcohols with CuL–Cl in aerated aqueous acetonitrile

The oxidative activity of CuL–Cl was probed in water/acetonitrile at room temperature, using benzyl alcohol as a model substrate. The addition of ^{t}BuOK has been essential for the alcohol activation. Other bases like NaOH and KOH can also be employed. The base has to be added after the alcohol in the exact stoichiometric amount and not in an excess that retards the reaction. The complex CuL–Cl enters the reaction mixture after the base to avoid a decrease of the catalyst efficiency. A similar behaviour for the GOase was noted by Hamilton et al. [64]. The activity of the GOase increased 20–30 times in the presence of oxidants such as hexacyanidoferrate(III), hexachloridoiridate(IV) or a Mn(III) edta complex. Conversely, the alcohol oxidation was completely inhibited in the presence of hexacyanidoferrate [64]. The reaction also did not occur under argon, while benzaldehyde was smoothly produced in air. The reaction rate further increased after air had been

Table 3
CuL–Cl mediated oxidation of selected primary alcohols under stoichiometric conditions.[a]

Entry	Alcohol	Conv.[b] (%)	Conv.[c] (%)	Conv.[d] (%)
1	Benzyl alcohol	15	45	92
2	Crotyl alcohol	18	56	90
3	Geraniol	32	78	95
4	4-Hydroxy-3-methoxy-benzyl alcohol	7	23	65
5	1-Octanol	21	56	87

[a] In the presence of 2 mmol of primary alcohol activated by 2 mmol of ^{t}BuOK and 2 mmol of CuL–Cl in CH_3CN/H_2O at room temperature. Reaction conditions are given in Section 2.
[b] Products analysed after 1 h.
[c] Products analysed after 3 h.
[d] Products analysed after 8 h.

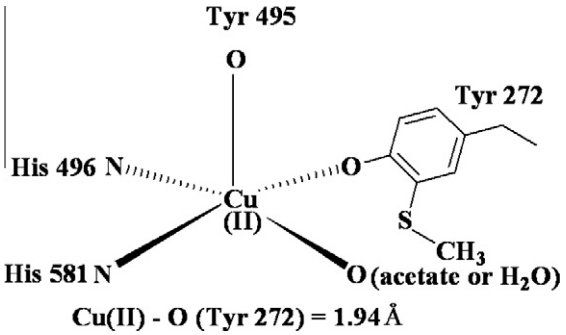

Fig. 10. Schematic representation of the active site of the GOase enzyme [11].

replaced by neat dioxygen. Using these conditions, with CuL–Cl we could oxidised a series of primary alcohols stoichiometrically to the corresponding aldehydes (Table 3). No reactivity of CuL–Cl towards secondary alcohols was observed.

When different copper(II) salts and Hpyrimol or Hpyramol are used in situ as catalyst precursors (see Section 2), the rate increases in the following order: $CuBr_2 > CuCl_2 > Cu(ClO_4)_2 > Cu(BF_4)_2 > Cu(NO_3)_2$. It is noteworthy that the oxidation catalyst formed in situ from $CuCl_2$ and Hpyramol/Hpyrimol gives results comparable to those obtained with the crystallized sample of CuL–Cl. When carrying out the oxidations at different temperatures, the reactivity increases in the order: 60 °C > 40 °C > 20 °C. At 90 °C, however, the reaction is slower than at 20 °C, indicating some instability of the catalyst above 60 °C. Good to excellent conversions were achieved with the various primary alcohols used which were deprotonated with ^{t}BuOK initially for their activation (Table 3). The active benzyl alcohol, crotyl alcohol and geraniol (entries 1–3) were almost completely converted to the corresponding aldehydes. The lower conversion reached with 4-hydroxy-3-methoxy-benzyl alcohol (entry 4) is most likely due to the deactivating character of the *p*-hydroxy substituent; nevertheless, 65% of vanillin resulted after a reaction time of 8 h. The selective oxidation of 1-octanol to 1-octanal is remarkable. Indeed, non-activated linear alkyl alcohols are known to be difficult to oxidise [65]. With CuL–Cl, a conversion of 87% was obtained (entry 5), which was comparable to the conversions achieved for the activated alcohols in entries 1–3. Moreover, no traces of the overoxidised octanoic acid were detected by gas chromatography.

3.8. CuL–Cl as a functional model of the GOase

The active site of the galactose oxidase (Fig. 10) is rather unusual, as the coordinated phenolate ligands (Tyr272 and Tyr495) together with a copper ion are involved in two-electron transfer catalysis. The modelling of this active site requires assembling a variety of functional groups in a specific geometric arrangement. The neutral complex CuL–Cl and its oxidised form can be considered as models of the native enzyme GOase with regard to the coordination environment of Cu(II). Similar to the GOase, the oxidation of the pyrimol ligand in CuL–Cl leads to a biradical complex in a singlet ground state ($S = 0$). The comparison of the antiferromagnetic coupling and stabilization of the singlet ground state ($S = 0$) in the oxidised GOase and $[CuL^{\cdot}–Cl(solvent)]^+$ would require qualitative analysis of the relative orientations and overlap of the magnetic orbitals of the Cu(II) centre and the phenoxyl radical $L^{\cdot}$ according to the Goodenough-Kanamori rules for exchange coupling [66]. Unfortunately, the crystal structure of $[CuL^{\cdot}–Cl(solvent)]^+$ could not be determined and the optimised geometry of the singlet oxidised state based on a reliable theoretical description of its electronic structure is currently not available (see above).

The Cu(II) centre in CuL–Cl is coordinated by a phenolate moiety (part of the tridendate pyrimol ligand) which closely resembles the Tyr272 moiety in the GOase. The pyrimol ligand is coordinated to Cu(II) in a nearly perfect square-planar environment and the bond distances in the plane match closely to those found at the GOase active site. In particular, the Cu–O1 distance in the equatorial plane is 1.94 Å, both in CuL–Cl and the GOase [67].

In the GOase, Tyr272, His496, His581 and the acetate ion from the crystallization buffer also form an almost perfect square. A fifth ligand, i.e. Tyr495, occupies the axial position at a longer distance than Tyr272 (Fig. 10). The four-coordinate Cu(II)–pyrimol compound features a strong rigidity brought in by the tridentate pyrimol ligand. Pyrimol forms two five-membered chelate rings, Cu1–N2–C21–C22–O1 and Cu1–N2–C1–C11–N1, thereby stabilizing the square-based geometry and preventing large structural changes induced by the oxidation of the phenolate moiety (as suggested by the spectro-electrochemical and computational studies). The rigid square-planar coordination is most likely crucial for the activity, being ensured by the protein backbone for the natural enzyme. In the $[CuL^{\cdot}–Cl(MeCN)]^+$ coordination sphere, the chloride ligand may act as a facile leaving group in the presence of alcoholate. The likely solvent-assisted replacement of the chloride in the equatorial plane by the deprotonated alcoholate species is favourable for a five-membered cyclic transition state (Fig. 11) and for the facile α-hydrogen abstraction as the key step in the alcohol oxidation, in contrast to alcoholate attachment in the axial position [68]. Importantly, the alcoholate oxidation is faster when $CuBr_2$ is used instead of $CuCl_2$ (see above), which provides an indirect evidence that the halide ligand indeed acts as a good leaving group for the alcoholate substrate.

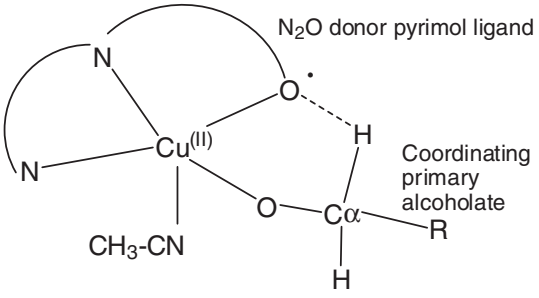

Fig. 11. The five-membered cyclic transition state involving $[CuL^{\cdot}–Cl(MeCN)]^+$, proposed for the α-hydrogen abstraction during primary alcohol oxidation.

4. Conclusions

The copper(II)–pyrimol compound (CuL–Cl) is capable of oxidising a series of primary alcohols to the corresponding aldehydes, under stoichiometric condition. The presence of dioxygen and ^{t}BuOK is essential for the oxidation process. The rigid square-planar coordination, owing to the double-chelating conjugated pyrimol ligand, appears to stabilize the singlet ground state ($S = 0$), on the phenoxyl radical formation. This geometry is also expected to assist the α-hydrogen abstraction from the alcoholate substrate through a five-membered cyclic transition state. The results of the spectro-electrochemical studies in dichloromethane and acetonitrile are indicative of a preserved chemical composition and square-planar geometry of the CuL–Cl moiety after the oxidation of the phenolate group, with a likely axial coordination of the donor solvent (acetonitrile, water). DFT and time-dependent DFT calculations provide a valuable insight into the molecular orbitals involved in the intraligand (L) and charge-transfer visible electronic transitions in CuL–Cl and its oxidised state.

The CuL–Cl complex is an effective bioinspired example of the aerobic oxidation of primary alcohols, bearing close resemblance to the native GOase enzyme. Functionally, some differences exist due to the rigid planar coordination of the single pyrimol ligand at Cu(II) and the flexible coordination of the separate amino acids in the innate enzyme. The likely catalytic activity of CuL–Cl presents a challenge for future studies.

Acknowledgements

This research was financially supported by the Dutch Economy, Ecology and Technology (EET) programme, a joint programme of the Ministry of Economic Affairs, the Ministry of Education, Culture and Science, and the Ministry of Housing, Spatial Planning and the Environment. M.L. and A.L.S. acknowledge financial support of the Netherlands Organization for Scientific Research (NWO-CW). Dr. Paul Alsters (DSM, Pharmaceuticals) and Dr. Ronald Hage (Unilever) are gratefully acknowledged for fruitful discussions. Dr. Roberta Pievo and Dr. Ilaria Gamba are thanked for recording and reproducing the EPR spectrum. The use of supercomputer facilities was sponsored by the Stichting Nationale Computerfaciliteiten (NCF), with a support from NWO-CW.

Appendix A. Supplementary material

CCDC 629865 and 629866 contain the supplementary crystallographic data for this paper. These data can be obtained free of charge from The Cambridge Crystallographic Data Centre via www.ccdc.cam.ac.uk/data_request/cif. Supplementary data associated with this article can be found, in the online version, at doi:10.1016/j.ica.2011.03.029.

References

[1] C.D. Borman, C.G. Saysell, A. Sokolowski, M.B. Twitchett, C. Wright, A.G. Sykes, Coord. Chem. Rev. 192 (1999) 771.
[2] P. Chaudhuri, K. Wieghardt, Prog. Inorg. Chem. 50 (2001) 151.
[3] P. Chaudhuri, K. Wieghardt, T. Weyhermuller, T.K. Paine, S. Mukherjee, C. Mukherjee, Biol. Chem. 386 (2005) 1023.
[4] S. Itoh, M. Taki, S. Fukuzumi, Coord. Chem. Rev. 198 (2000) 3.
[5] B.A. Jazdzewski, W.B. Tolman, Coord. Chem. Rev. 200 (2000) 633.
[6] F. Thomas, Eur. J. Inorg. Chem. (2007) 2379.
[7] S.K. Alamsetti, S. Mannam, P. Mutupandi, G. Sekar, Chem. Eur. J. 15 (2009) 1086.
[8] A. John, M.M. Shaikh, P. Ghosh, Dalton Trans. (2008) 2815.
[9] L. Que, W.B. Tolman, Nature 455 (2008) 333.
[10] C. Mukherjee, U. Pieper, E. Bothe, V. Bachler, E. Bill, T. Weyhermuller, P. Chaudhuri, Inorg. Chem. 47 (2008) 8943.
[11] J.W. Whittaker, Chem. Rev. 103 (2003) 2347.
[12] B.P. Branchaud, M.P. Montaguesmith, D.J. Kosman, F.R. McLaren, J. Am. Chem. Soc. 115 (1993) 798.
[13] N. Ito, S.E.V. Phillips, C. Stevens, Z.B. Ogel, M.J. McPherson, J.N. Keen, K.D.S. Yadav, P.F. Knowles, Nature 350 (1991) 87.
[14] J. Stubbe, W.A. van der Donk, Chem. Rev. 98 (1998) 705.
[15] M.M. Whittaker, D.P. Ballou, J.W. Whittaker, Biochemistry 37 (1998) 8426.
[16] M.M. Whittaker, J.W. Whittaker, J. Biol. Chem. 263 (1988) 6074.
[17] S.G. Minasian, M.M. Whittaker, J.W. Whittaker, Biochemistry 43 (2004) 13683.
[18] M.M. Whittaker, J.W. Whittaker, Biochemistry 40 (2001) 7140.
[19] E. Bill, J. Muller, T. Weyhermuller, K. Wieghardt, Inorg. Chem. 38 (1999) 5795.
[20] F. Michel, F. Thomas, S. Hamman, E. Saint-Aman, C. Bucher, J.L. Pierre, Chem. Eur. J. 10 (2004) 4115.
[21] R.C. Pratt, T.D.P. Stack, Inorg. Chem. 44 (2005) 2367.
[22] J.G. Radziszewski, M. Gil, A. Gorski, J. Spanget-Larsen, J. Waluk, B.J. Mroz, J. Chem. Phys. 115 (2001) 9733.
[23] I. Sylvestre, J. Wolowska, C.A. Kilner, E.J.L. McInnes, M.A. Halcrow, Dalton Trans. (2005) 3241.
[24] M. Taki, H. Hattori, T. Osako, S. Nagatomo, M. Shiro, T. Kitagawa, S. Itoh, Inorg. Chim. Acta 357 (2004) 3369.
[25] R. Uma, R. Viswanathan, M. Palaniandavar, M. Lakshminarayanan, J. Chem. Soc., Dalton Trans. (1994) 1219.
[26] M. Vaidyanathan, M. Palaniandavar, R.S. Gopalan, Indian J. Chem., Sect. A: Inorg. Bioinorg. Phys. Theor. Anal. Chem. 42 (2003) 2210.
[27] C. Zondervan, R. Hage, B.L. Feringa, Chem. Commun. (1997) 419.
[28] P. Milko, J. Roithova, N. Tsierkezos, D. Schroder, J. Am. Chem. Soc. 130 (2008) 7186.
[29] D. Rokhsana, D.M. Dooley, R.K. Szilagyi, J. Biol. Inorg. Chem. 13 (2008) 371.
[30] J. Manzur, H. Mora, A. Vega, D. Venegas-Yazigi, M.A. Novak, J.R. Sabino, V. Paredes-Garcia, E. Spodine, Inorg. Chem. 48 (2009) 8845.
[31] N. Kitajima, K. Whang, Y. Morooka, A. Uchida, Y. Sasada, J. Chem. Soc., Chem. Commun. (1986) 1504.
[32] Y.D. Wang, T.D.P. Stack, J. Am. Chem. Soc. 118 (1996) 13097.
[33] P. Chaudhuri, M. Hess, U. Florke, K. Wieghardt, Angew. Chem., Int. Ed. 37 (1998) 2217.
[34] P. Chaudhuri, M. Hess, J. Muller, K. Hildenbrand, E. Bill, T. Weyhermuller, K. Wieghardt, J. Am. Chem. Soc. 121 (1999) 9599.
[35] J.S. Panek, C.E. Masse, Angew. Chem., Int. Ed. 38 (1999) 1093.
[36] Y.D. Wang, J.L. DuBois, B. Hedman, K.O. Hodgson, T.D.P. Stack, Science 279 (1998) 537.
[37] R. Behrendt, C. Renner, M. Schenk, F.Q. Wang, J. Wachtveitl, D. Oesterhelt, L. Moroder, Angew. Chem., Int. Ed. 38 (1999) 2771.
[38] S. Itoh, S. Takayama, R. Arakawa, A. Furuta, M. Komatsu, A. Ishida, S. Takamuku, S. Fukuzumi, Inorg. Chem. 36 (1997) 1407.
[39] A. Philibert, F. Thomas, C. Philouze, S. Hamman, E. Saint-Aman, J.L. Pierre, Chem. Eur. J. 9 (2003) 3803.
[40] E. Zueva, P.H. Walton, J.E. McGrady, Dalton Trans. (2006) 159.
[41] P.U. Maheswari, S. Roy, H. den Dulk, S. Barends, G. van Wezel, B. Kozlevcar, P. Gamez, J. Reedijk, J. Am. Chem. Soc. 128 (2006) 710.
[42] L.D. Pachon, A. Golobic, B. Kozlevcar, P. Gamez, H. Kooijman, A.L. Spek, J. Reedijk, Inorg. Chim. Acta 357 (2004) 3697.
[43] Y.L. Wong, D.K.P. Ng, H.K. Lee, Inorg. Chem. 41 (2002) 5276.
[44] A.J.M. Duisenberg, L.M.J. Kroon-Batenburg, A.M.M. Schreurs, J. Appl. Crystallogr. 36 (2003) 220.
[45] G.M. Sheldrick, Acta Crystallogr., Sect. A 64 (2008) 112.
[46] A.L. Spek, J. Appl. Crystallogr. 36 (2003) 7.
[47] G.M. Sheldrick, University of Göttingen, Germany, 1999.
[48] P.T. Beurskens, G. Admiraal, G. Beurskens, W.P. Bosman, S. Garcia-Granda, R.O. Gould, J.M.M. Smits, C. Smykalla, The DIRDIF Program System, Technical Report of the Crystallography Laboratory, University of Nijmegen, The Netherlands, 1999.
[49] R. Herbst-Irmer, G.M. Sheldrick, Acta Crystallogr., Sect. B 54 (1998) 443.
[50] R.C. Pratt, T.D.P. Stack, J. Am. Chem. Soc. 125 (2003) 8716.
[51] E.A. Boudreaux, L.N. Mulay, Theory and Applications of Molecular Magnetism, John Wiley & Sons, New York, 1976.
[52] F. Hartl, R.P. Groenestein, T. Mahabiersing, Collect. Czech. Chem. Commun. 66 (2001) 52.
[53] M. Krejčík, M. Daněk, F. Hartl, J. Electroanal. Chem. 317 (1991) 179.
[54] T. Mahabiersing, H. Luyten, R.C. Nieuwendam, F.E. Hartl, Collect. Czech. Chem. Commun. 68 (2003) 1687.
[55] F. Hartl, H. Luyten, H.A. Nieuwenhuis, G.C. Schoemaker, Appl. Spectrosc. 48 (1994) 1522.
[56] J.A. Pople, GAUSSIAN 03, Revision C.02, Gaussian, Inc., Wallingford, CT, 2004.
[57] P.J. Stephens, F.J. Devlin, C.F. Chabalowski, M.J. Frisch, J. Phys. Chem. 98 (1994) 11623.
[58] A.D. Becke, J. Chem. Phys. 98 (1993) 5848.
[59] J. Tomasi, B. Mennucci, R. Cammi, Chem. Rev. 105 (2005) 2999.
[60] F. Hartl, Inorg. Chim. Acta 232 (1995) 99.
[61] J.A. Halfen, V.G. Young, W.B. Tolman, Angew. Chem., Int. Ed. 35 (1996) 1687.
[62] R. van Gorkum, E. Bouwman, J. Reedijk, 43 (2004) 2456.
[63] L. Benisvy, E. Bill, A.J. Blake, D. Collison, E.S. Davies, C.D. Garner, G. McArdle, E.J.L. McInnes, J. McMaster, S.H.K. Ross, C. Wilson, Dalton Trans. (2006) 258.
[64] G.A. Hamilton, P.K. Adolf, J. Dejersey, G.C. Dubois, G.R. Dyrkacz, R.D. Libby, J. Am. Chem. Soc. 100 (1978) 1899.
[65] D. Geisslmeier, W.G. Jary, H. Falk, Monatsh. Chem. 136 (2005) 1591.
[66] J. Muller, T. Weyhermuller, E. Bill, P. Hildebrandt, L. Ould-Moussa, T. Glaser, K. Wieghardt, Angew. Chem., Int. Ed. 37 (1998) 616.
[67] N. Ito, S.E. Phillips, K.D. Yadav, P.F. Knowles, J. Mol. Biol. 238 (1994) 794.
[68] A. Kohen, J.P. Klinman, Chem. Biol. 6 (1999) R191.